IEICE TRANSACTIONS

on Electronics

DOI:10.1587/transele.2024ECP5023

Publicized:2024/08/26

This advance publication article will be replaced by the finalized version after proofreading.

A PUBLICATION OF THE ELECTRONICS SOCIETY

The Institute of Electronics, Information and Communication Engineers
Kikai-Shinko-Kaikan Bldg., 5-8, Shibakoen 3chome, Minato-ku, TOKYO, 105-0011 JAPAN

PAPER

A Study on Optimal Design of Magneto-Metasurface for THz Isolator

Mio TANIGUCHI[†], ***Student Member***, **Akito IGUCHI**[†], ***Member***, ***and*** **Yasuhide TSUJI**[†a)], ***Senior Member***

SUMMARY In this paper, we design one-dimensional (1D) magneto-metasurface for THz isolator application. In this optimization, frequency domain finite element method (FD-FEM) with periodic boundary condition (PBC) is employed as a numerical simulation method and two kinds of evolutionary algorithms were used to optimize design parameters. In order to optimize two objectives to maximize unidirectional transmission and isolation ratio, we propose a novel objective function using ELU function. The results show that designed metasurface isolator with relatively simple structure can realize unidirectional transmission. In addition, it is demonstrated that angular characteristics is improved by optimizing DC magnetic field and operating temperature.
key words: *metasurface, magnetic material, THz band, isolator, optimal design*

1. Introduction

Metamaterials are attracting a lot of attention because they can realize unique properties that cannot be achieved with ordinary materials, such as, negative refractive index [1], [2]. Especially, a lot of applications of metasurface have been reported, such as, meta-holograms [3], [4], metalenses [5], [6], invisibility cloaks [7]–[11] and intelligent reflecting surfaces (IRS)[12], and so on[13]–[15], because metasurface with two-dimensional (2D) structure is easy to be fabricated by existing semiconductor fabrication process compared to three-dimensional metamaterials. Isolator is one of the important components in various applications and isolators utilizing magnetic/nonmagnetic metasurface have been reported [16], [17]. We consider isolator because of their important roles in source protection, impedance matching, noise canceling, and decoupling. S. Chen, *et al.* have successfully developed isolator by utilizing asymmetric structure in 2D surface. However, structures with cylindrical rods may be difficult to fabricate with sufficient precision because the large nonreciprocity is achieved utilizing resonance effect between rods. Our proposed structure utilize asymmetry of the arrangement of SiO_2 and InSb to obtain large nonreciprocity. Therefore, fabrication tolerance and the resulting angular characteristics is expected be improved. On the other hand, the isolator proposed by Z. Tan, *et al.* has 1D periodic structure and seems to be easy to fabricate compared to the isolator proposed by S. Chen, *et al.*, however, the isolation ratio of this isolator is about only 13 dB.

[†]Graduate School of Engineering, Muroran Institute of Technology, 27-1 Mizumoto-cho, Muroran, Hokkaido 050-8585, Japan
a) E-mail: y-tsuji@muroran-it.ac.jp

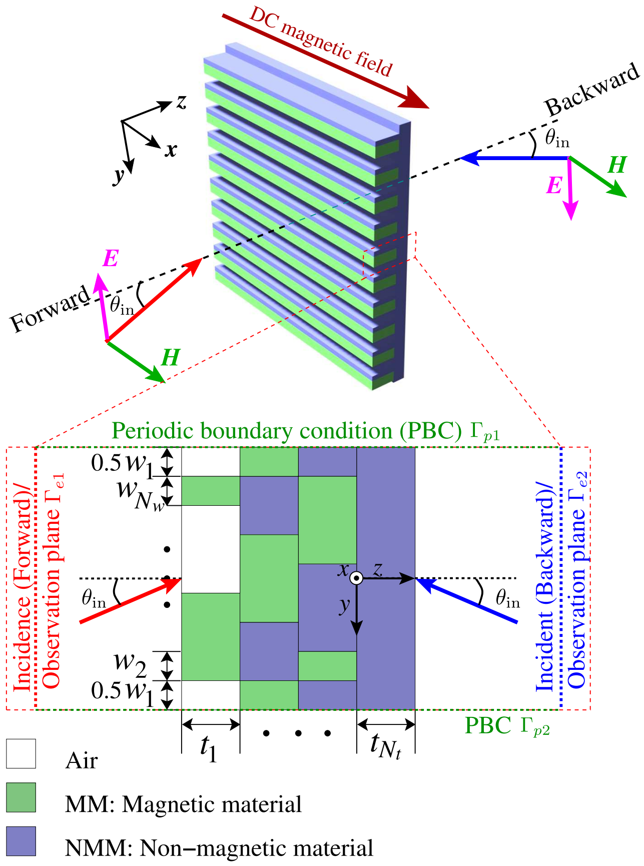

Fig. 1: Magneto-metasurface isolator with 1D periodic structure.

In this paper, we design metasurface isolator with simple 1D structure consists of InSb and SiO_2 [18] to improve isolator characteristics. In this design, we employ frequency domain finite element method (FD-FEM) with periodic boundary condition (PBC) [19], [20] to calculate transmission characteristics and harmony search algorithm (HSA) [21], [22] and genetic algorithm (GA) [23]–[25] to optimize design variables. In order to realize high transmission and high isolation ratio simultaneously, a novel objective function using nonlinear exponential linear unit (ELU) function is used [26].

In Section 2, we briefly describe our design strategy of metasurface isolator. In Section 3, we show some design examples and give some discussion about basic structure and objective function to improve isolator characteristics. Finally, in Section 4, we conclude the findings in this paper.

2. Design of One-Dimensional Magneto-Metasurface

2.1 Basic structure of metasurface isolator

A schematic view of a 1D metasurface isolator is shown in Fig. 1. DC magnetic field is applied along x-direction and isolation of forward and backward propagation of y-polarized THz wave is considered. The unit cell of metasurface is depicted in the inset and has asymmetric structure along y-direction. In this paper, InSb is used as a magneto-optic material [27], [28] and SiO_2 is used as a substrate. SiO_2 is also used to realize asymmetric structure. The relative permittivity of InSb is expressed as the following tensor form [16]:

$$[\varepsilon_{\mathrm{InSb}}] = \begin{bmatrix} \varepsilon_{xx} & 0 & 0 \\ 0 & \varepsilon_{yy} & \varepsilon_{yz} \\ 0 & -\varepsilon_{yz} & \varepsilon_{zz} \end{bmatrix} \tag{1}$$

$$\varepsilon_{xx} = \varepsilon_\infty - \frac{\omega_p^2}{\omega(\omega + j\gamma)}, \quad \varepsilon_{yz} = \frac{-j\omega_p^2\omega_c}{\omega\{(\omega + j\gamma)^2 - \omega_c^2\}},$$

$$\varepsilon_{yy} = \varepsilon_{zz} = \varepsilon_\infty - \frac{\omega_p^2(\omega + j\gamma)}{\omega\{(\omega + j\gamma)^2 - \omega_c^2\}},$$

where $\varepsilon_\infty = 15.68$ is the high-frequency limit permittivity. $\omega_p = (Ne^2/\varepsilon_0 m^*)^{1/2}$ and $\omega_c = eB/m^*$ are the plasma and cycrotron angular frequency, respectively, where e is the electron charge, ε_0 is the free-space permittivity, and B is the applied DC magnetic field. $m^* = 0.015m_e$ is the effective mass of the carrier for the InSb where m_e is the electron mass. N is the intrinsic carrier density and is expressed as follows:

$$N(\mathrm{cm}^{-3}) = 5.76 \times 10^{14} T^{1.5} \exp\left[\frac{-0.26}{2 \times 8.625 \times 10^{-5} \times T}\right] \tag{2}$$

where T is the temperature. Therefore, permittivity tensor for the InSb depends on B and T. We consider the basic structure as a combination of rectangle blocks. The design variables, w_i $(i = 1 \sim N_w)$ and t_j $(j = 1 \sim N_t)$ in Fig 1, are optimized by HSA or GA. By increasing the values of N_w and N_t, various structures can be designed. The search range of each design variable is set to $5 \le w_i/\mu\mathrm{m} \le 40$ and $10 \le t_j/\mu\mathrm{m} \le 200$, respectively. When magnetic material with a DC magnetic field applied in the x direction is considered, the wave equation is expressed as follows:

$$\frac{\partial}{\partial y}\left[\frac{1}{\sigma}\left(\varepsilon_{yy}\frac{\partial H_x}{\partial y} - \varepsilon_{yz}\frac{\partial H_x}{\partial z}\right)\right] + \frac{\partial}{\partial z}\left[\frac{1}{\sigma}\left(\varepsilon_{zz}\frac{\partial H_x}{\partial z} - \varepsilon_{zy}\frac{\partial H_x}{\partial y}\right)\right] + k_0^2 H_x = 0 \tag{3}$$

where $\sigma = \varepsilon_{yy}\varepsilon_{zz} + \varepsilon_{yz}\varepsilon_{yz}$, k_0 is a free-space wavenumber. We assume that the applied DC magnetic field affects only the relative permittivity tensor and only high frequency component is considered in H_x. The analysis domain is discretized using second-order triangular nodal elements and FD-FEM is applied to (3). The analytical solutions are connected to Γ_{e1} and Γ_{e2} (xy-plane) in Fig. 1, and PBC is applied between Γ_{p1} and Γ_{p2}(xz-plane)[19]. Evolutionary methods, HSA and GA, are used for size optimization. HSA and GA are explained in the Appendix.

2.2 Optimization for multi-objective

In the design of isolators, it is necessary to maximize both isolation ratio and one-way transmission. Therefore it is required to optimize two or more different objectives simultaneously. For this reason, we introduce the ELU function, which is a nonlinear function, to define the objective function in this paper. At the first, the optimization behaviors when using objective function based on weighted sum and nonlinear ELU function are compared. The objective function usually used for multi-objective is expressed as follows:

$$\text{Minimize } C_{\mathrm{OF1}} = \sum_{i=1}^{2}(\alpha_i C_i) \tag{4}$$

where C_1 and C_2 are objective functions for maximizing isolation ratio and transmittance, respectively. α_1 and α_2 are weighting factor for each objective. Figure 2(a) shows the color contour of C as a function of C_1 and C_2. Minimum target property ($C_1 < 0$ and $C_2 < 0$) is shown by thick solid line and search directions for different start points (P_1, P_2, P_3) are illustrated. The objective function is negative in the hatched area, however, C_1 or C_2 have positive value and minimum requirement is not satisfied. Therefore, we introduce the ELU function to determine the objective function for multi-objective as follows:

$$\text{Minimize } C_{\mathrm{OF2}} = \sum_{i=1}^{2}\mathrm{ELU}(\alpha_i C_i) \tag{5}$$

$$\mathrm{ELU}(x) = \begin{cases} x & (x \ge 0) \\ e^x - 1 & (x < 0) \end{cases} \tag{6}$$

Figure 2(b) shows the color contour of C as a function of C_1 and C_2. We can see that the objective with poor characteristics is improved more. The usefulness of the ELU function is discussed in detail in the Appendix.

3. Design Examples of Metasurface Isolator

3.1 Single frequency design

First, we will demonstrate the effect of the objective function using the basic model, and then we will discuss whether operation bandwidth can be expanded by increasing the design parameters. We consider magneto-metasurface shown in Fig. 1 and non-magnetic material (NMM), magnetic material (MM), and surroundings are assumed to be SiO_2,

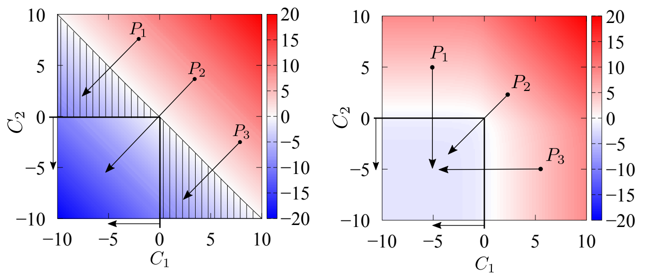

(a) Weighted sum (b) ELU function

Fig. 2: Color contour of objective function distribution and search directions at different points ($\alpha_1 = \alpha_2 = 1$).

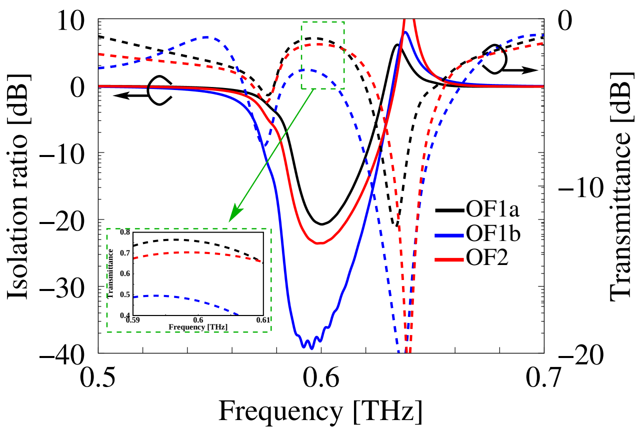

Fig. 3: Transmission and isolation ratio properties of magneto metasurface designed at 0.6 THz. OF1a and OF1b denote OF1 with $(\alpha_1, \alpha_2) = (1, 5)$, and $(1, 1000)$, respectively.

InSn, and air, respectively. Air and SiO_2 are assumed to be isotropic nondispersive media and their relative permittivities are set to be $\varepsilon_{\text{air}} = 1$ and $\varepsilon_{SiO_2} = 4$. InSb has a magneto-optical effect and its permittivity tensor is expressed by Eq. (1) [16]. The operating frequency is set to be $f = 0.6$ THz and the normal incidence ($\theta_{\text{in}} = 0$) is assumed. the temperature is set to be $T = 230$ K and the applied DC magnetic field is set to be $B = 0.4$ T. The design variables in this optimization are w_1, w_2, w_3, t_1, and t_2. These values are optimized by HSA.

First, in order to discuss the difference in optimal design results depending on the objective function, we consider two kinds of objective functions as follows:

- OF1 defined as Eq. (4) :

$$\begin{cases} C_1 = -T_f, \ C_2 = T_b & (T_f > T_b) \\ C_1 = -T_b, \ C_2 = T_f & (T_f < T_b) \end{cases} \tag{7}$$

  where T_f and T_b are the transmittance when the incidence are from $z = -\infty$ and $+\infty$, respectively, and in this paper, we call these as forward and backward transmittance, respectively. In this objective function, we aim to achieve one-way transmission in either $+z$ or $-z$-direction. If we want to obtain one-way transmission in the opposite direction, that can be achieved by changing the front and back side of the metasurface. To achieve one-way transmission, smaller C_1 and smaller C_2 are aimed.
- OF2 defined as Eq. (5):

$$C_1 = T_{\text{aim}} - T_b \tag{8}$$

$$C_2 = 1 - \frac{\text{IR}}{\text{IR}_{\text{aim}}}, \qquad \text{IR} = 10 \log_{10} \frac{T_b}{T_f} \tag{9}$$

where T_{aim} and IR_{aim} represent minimum required backward transmittance and isolation ratio (IR), respectively. In this case, we define the transmission direction as the backward direction based on the design results using OF1. We consider different C_1 and C_2 in OF1 and OF2. C_2 is possible to be $\simeq -\infty$ when IR increases to be ∞, then only C_2 may be improved if Eq. (9) is used in OF1. On the other hand, $\text{ELU}(C_2)$ is larger than -1 if $C_2 = -\infty$. This is the reason why we employ OF2.

Figure 3 shows the transmission and isolation ratio properties of the optimally designed metasurface isolators. In OF1, two sets of $(\alpha_1, \ \alpha_2) = (1, 5), \ (1, 1000)$ are used. In OF2, $(\alpha_1, \ \alpha_2)$ are set to be $(50, 20)$ and T_{aim} and IR_{aim} is set to be 0.65 and -20 dB, respectively. When using OF1 with $(\alpha_1, \ \alpha_2) = (1, 5)$, transmittance in pass direction achieve 0.76 at $f = 0.6$ THz and IR slightly exceed -20 dB within narrow spectral range. When using OF1 with $(\alpha_1, \ \alpha_2) = (1, 1000)$, higher IR of 38 dB is obtained, however, transmittance is significantly degraded to 0.43. Therefore, we can see that weighting factor $(\alpha_1, \ \alpha_2)$ has to be carefully determined. On the other hand, the isolator designed using OF2 achieve transmittance of 0.7 and IR of 23.5 dB at $f = 0.6$ THz and both requirements of transmittance and IR are satisfied within wider frequency range.

3.2 Design for broadband operation

In order to expand the operation bandwidth, we consider three types of unit cell structures, as shown in Fig. 4. The design variables are w_i $(i = 1 \sim N_w)$, t_j $(j = 1 \sim N_t)$ and these values are optimized by GA. In order to achieve one-way transmission, an asymmetric arrangement of magnetic and non-magnetic materials is required so that the electromagnetic waves feel different structure with respect to the different direction of propagation. The simplest of these asymmetric structures is that of Fig. 4(a). Therefore, we employ this structure first. After that, the structures in Fig. 4(b) and (c) are considered to discuss if the characteristics can be improved by considering structures with a higher degree of freedom. Fig. 4(c) mimics trapezoidal structure. Figure 5 shows the results of size optimization at frequency of 0.6 THz using OF2 with $\alpha_1 = 50$, $\alpha_2 = 20$, $T_{\text{aim}} = 0.50$, and $\text{IR}_{\text{aim}} = 40$ dB. Only structure #2 and #3 achieve IR ≥ 40 dB and the structure #3 has better properties compared with the structure #1 and #2. The bandwidth in which IR ≥ 20 dB and $T_b \geq 0.5$ are satisfied is 32 GHz in the structure #3.

Next, in order to broaden operation bandwidth, we modify the objective function as follows:

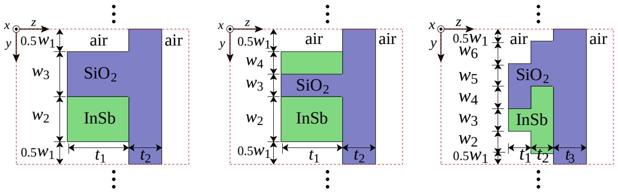

(a) Structure #1 ($N_w = 3,\ N_t = 2$) (b) Structure #2 ($N_w = 4,\ N_t = 2$) (c) Structure #3 ($N_w = 6,\ N_t = 3$)

Fig. 4: Basic unit cell considered in this paper.

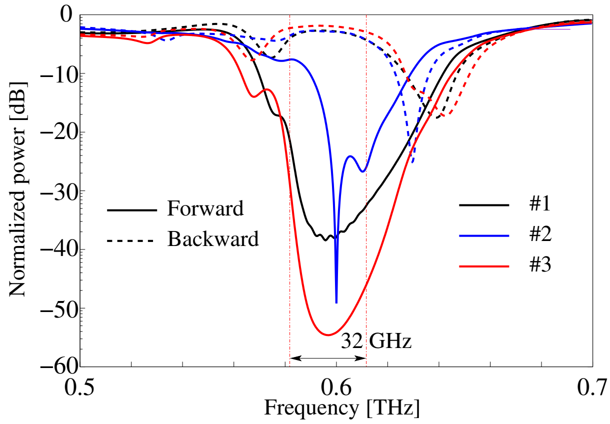

Fig. 5: Forward and backward transmission properties of magneto metasurface designed at 0.6 THz.

$$\text{Minimize } C_f = \max_{f \in \mathbf{F}} C(f), \tag{10}$$

$$\mathbf{F} = \{0.58,\ 0.59,\ 0.60,\ 0.61,\ 0.62 \text{ THz}\}$$

where C_f is defined by Eq. (10). In this optimization, requirement for IR is relaxed to $\text{IR}_{\text{aim}} = 20$ dB. Figure 6 shows the forward and backward transmission properties of the optimized magneto metasurface isolator. Bandwidth which satisfy IR ≥ 20 dB and $T_b \geq 0.5$ are 31.4 GHz, 18.4 GHz, and 35.0 GHz in the structure #1, #2, and #3, respectively. We can see that the operation bandwidth is improved by broadband optimization. Especially, the broader operation bandwidth is achieved in the structure #1 and #3.

3.3 Design for wide angle operation

Next, we design metasurface isolator which can work in wide angle range. In order to use metasurface isolator within the incidence angle of −40° ∼ 40°, we define the objective function as follows:

$$\text{Minimize } C_\theta = \max_{\theta_{\text{in}} \in \mathbf{\Theta}} \sum_{i=1}^{2} \text{ELU}(\alpha_i C_i) \tag{11}$$

$$\mathbf{\Theta} = \{-40^\circ, -20^\circ, 0^\circ, 20^\circ, 40^\circ\}$$

where θ_{in} is the incident angle in yz-plane. We consider the structure #1 and #3 and $\alpha_1 = 50$, $\alpha_2 = 20$, $T_{\text{aim}} = 0.7$ and $\text{IR}_{\text{aim}} = 20$ dB are used. In addition, we employ the HSA

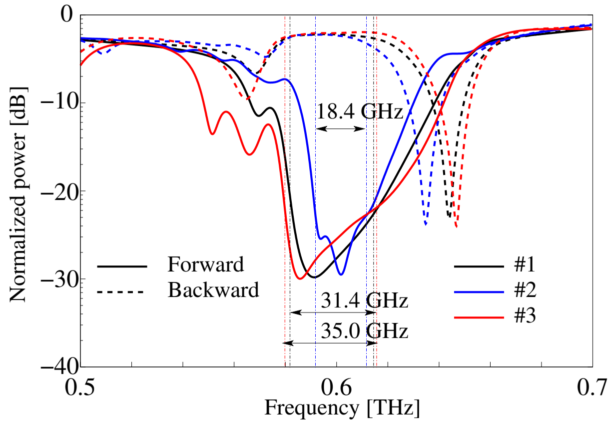

Fig. 6: Forward and backward transmission properties of magneto metasurface designed between 0.58 and 0.62 THz.

to optimize design variables because good search performance has been reported in [22]. The operation frequency is assumed to be $f = 0.6$ THz. Figure 7 shows the angular characteristics of the designed metasurface isolator at $T = 230$ K and $B = 0.4$ T. However, we can see that the angle dependence is large and the aimed characteristics are achieved only in a narrow angle range.

In order to improve the angular characteristics, we include the temperature and the DC magnetic field intensity into the design variables. We set the search range for these values as $210 \leq T/\text{K} \leq 250$, $-0.3 \leq B/\text{T} \leq 0.5$. We consider only the structure #1 because the performance is almost same for both #1 and #3 in Fig. 7. Figure 8 shows the results of the optimal design. We can see that the angular characteristics is greatly improved by tuning the temperature and the DC magnetic field intensity. Their optimized values are $B = 0.42$ T and $T = 232.75$ K and the optimized structural parameters are $w_1 = 10.9\ \mu$m, $w_3 = 17.9\ \mu$m, and $w_2 = 22.4\ \mu$m, $t_1 = 200\ \mu$m, and $t_2 = 99\ \mu$m. Figure 9 shows the propagation field in the case of the incidence angle of −40°, 0°, and 40°. It is seen that this metasurface works as an isolator in wide angle range. In this metasurface, reflected wave is not completely suppressed when incidence angle is large, therefore, interference between incidence and reflected wave is observed. However, we can see that the backward transmission is enough suppressed.

4. Conclusion

In this paper, we have designed 1D magneto-metasurfaces consist of InSb and SiO_2. In order to satisfy two different objectives simultaneously, we improved the objective function by using nonlinear function. In order to realize metasurface isolator, first, three kinds of basic structures were considered and their structural parameters were optimized in the normal incidence case. Then, in order to improve angular characteristics, we designed the structural parameters together with the temperature and the magnetic field intensity and achieved wide angle operation. We believe that the ELU based ob-

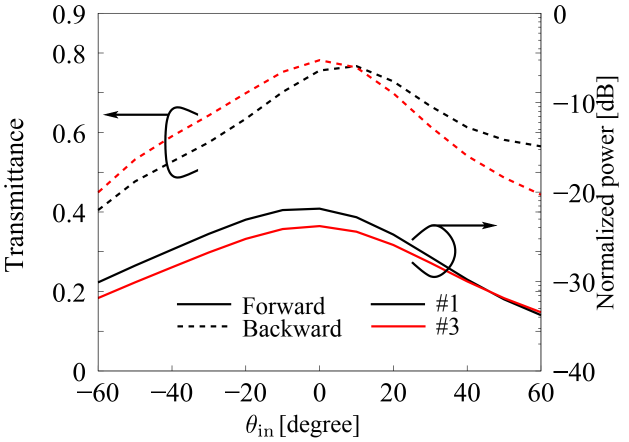

Fig. 7: Angular characteristics of magneto metasurface designed at 0.6 THz.

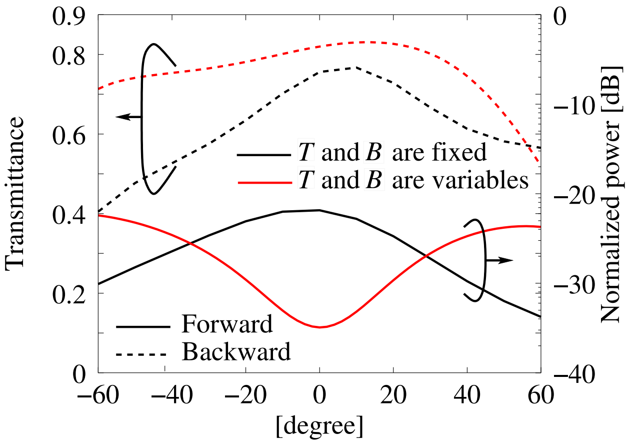

Fig. 8: Angular characteristics of magneto metasurface designed for wide angle operation

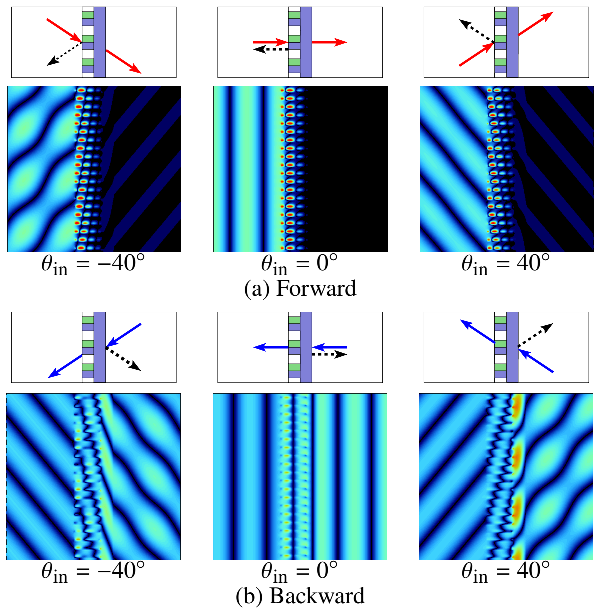

Fig. 9: Propagation field distribution in the case of plane wave incidence to the metasurface designed for wide angle operation.

jective function is effective regardless of the optimization method. In the future, we will apply topology optimal design [22], [29]–[31] to 2D metasurface design for achieving higher performance metasurfaces.

Acknowledgments

This research was supported by JST Next-Generation Researchers'Challenging Research Program JPMJSP2153 and JSPS Grants-in-Aid for Scientific Research 21K04169.

Appendix

A. Optimizatoin method

Harmony search is a scheme inspired by the improvisation process of jazz musicians. A new harmony is generated through selection and tuning process. Each design variable is selected from harmony memory, in which past relatively good harmonies are stored. The selected harmony is tuned or replaced by a random number with a certain probability. The new harmony x_h^{new} is generated as follows:

$$x_h^{\mathrm{new}} = \begin{cases} x_{i,\min} + (x_{i,\max} - x_{i,\min})C \\ \qquad\qquad (C_h \leq (1 - R_{\mathrm{hmer}})) \\ x_{p_i,i} + \Delta \qquad (C_h \leq (1 - R_{\mathrm{hmer}}) + R_{\mathrm{hmer}} R_{\mathrm{par}}) \\ x_{p_i,i} \qquad (\text{otherwise}) \end{cases} \tag{A-1}$$

where $C_h = U(0, 1)$, $C = U(0, 1)$, $\Delta = \alpha_{\mathrm{BW}} U(-1, 1)$, R_{hmer} is a harmony memory considering rate, R_{par} is a pitch adjusting rate, and α_{BW} is a bandwidth. $U(a, b)$ is a function which returns a random number in [0, 1], $x_{i,\min}$ and $x_{i,\max}$ are the minimum and maximum values of the i-th design variable, respectively. In the following optimization, $R_{\mathrm{hmer}} = 0.98$, $R_{\mathrm{par}} = 0.3$ is used, and α_{BW} is determined by difference value between arbitrary selected two harmonies [22].
Genetic Algorithm (GA) is one of popular evolutionary approaches and is widely used. In addition, various types of variants have been developed so far. GA is based on genetic process, such as, crossover between selected parents and mutation. In this paper, both elite selection and ranking selection are employed to select parents. From the selected parents (x_{p1}, x_{p2}), the i-th design variable of children (x_c) in the next generation is generated as follows:

$$x_{c,i} = \begin{cases} C x_{p1,i} + (1 - C) x_{p2,i} & (C_m \leq R_m) \\ x_{i,\min} + (x_{i,\max} - x_{i,\min})C & (\text{otherwise}) \end{cases} \tag{A-2}$$

where $C_m = U(0, 1)$, and R_m is a mutation rate, R_m is set to be $R_m = 0.03$ in the following optimization [22].

B. Objective function

Here, the objective functions OF1 and OF2 are discussed in detail. First, we consider C_{OF1} written as follows :

$$C_{\mathrm{OF1}} = -\alpha_1 T_p + \alpha_2 T_s \qquad \text{(B-1)}$$

where T_p and T_s are the transmittance in the pass and stop directions, respectively. As an example, we consider the case where the desired property is (T_p, IR) = (0.7, 20 dB) and let the value of C_{OF1} with (T_p, IR) = (0.7, 20 dB) is denoted by C^*_{OF1}. Table 1 shows some examples of the transmission properties with C_{OF1} smaller than C^*_{OF1} for several values of α_1 and α_2. From Table 1, it can be seen that even for a smaller C_{OF1} than C^*_{OF1}, the characteristics is possible to be much lower than the target value.

Table 1: Values of C_{OF1} for some cases of (α_1, α_2).

(α_1, α_2)	T_p	T_s	IR [dB]	C_{OF1}	C^*_{OF1}
(10,1)	0.72	0.2	5.56	-7.0	-6.993
(1,1)	0.73	0.03	13.86	-0.7	-0.693
(1,10)	0.65	0.002	25.12	-0.63	-0.630
(1,100)	0.50	0.005	20.00	0.0	0.000
(1,1000)	0.20	0.0065	14.88	6.3	6.300

C^*_{OF1} is the value of C_{OF1} with (T_p, IR) = (0.7, 20 dB).

Next, we consider C_{OF2} written as follows :

$$C_{\mathrm{OF2}} = \alpha_1 (T_{\mathrm{aim}} - T_p) + \alpha_2 (1 - \mathrm{IR}/\mathrm{IR}_{\mathrm{aim}}) \qquad \text{(B-2)}$$

where $T_{\mathrm{aim}} = 0.7$, $\mathrm{IR}_{\mathrm{aim}} = 20$ dB, respectively. In this case, the value of C_{OF2} is $C^*_{\mathrm{OF2}} = 0$ when the desired property is satisfied. Table 2 shows the value of C_{OF2} for the same transmission characteristics as in Table 1 when $(\alpha_1, \alpha_2) =$ (50,20). As is clear from Table 2, the value of C_{OF2} is far larger than C^*_{OF2}. Therefore, it is seen that these unacceptable transmission characteristics are correctly distinguished.

Table 2: Values of C_{OF2} for the same transmission properties as in Table 1.

(α_1, α_2)	T_p	T_s	IR [dB]	C_{OF2}	C^*_{OF2}
(50,20)	0.72	0.2	5.56	13.8	0.0
(50,20)	0.73	0.03	13.86	5.36	0.0
(50,20)	0.65	0.002	25.12	1.51	0.0
(50,20)	0.50	0.005	20.00	10.0	0.0
(50,20)	0.20	0.0065	14.88	30.1	0.0

C^*_{OF2} is the value of C_{OF2} with (T_p, IR) = (0.7, 20 dB).

Table 3 shows some transmission properties when $C_{\mathrm{OF2}} \simeq 0$. It can be seen that even if one characteristic greatly exceeds the target property, the degradation of the other characteristic from the target value has to be very small. From these discussions, the proposed objective function C_{OF2} is thought to be superior to C_{OF1} in the present multi-objective design. The difference of C_{OF1} and C_{OF2} is also illustrated in Fig. 2. By the way, to ensure that the target property is always satisfied when $C_{\mathrm{OF2}} = 0$, the ELU function should be replaced with the ReLU (Rectified Linear Unit) function. However, in that case, $C_{\mathrm{OF2}} = 0$ for both (T_p, IR) = (1.0, 30 dB) and (0.7, 20 dB). It is obvious that the former is better. Therefore, the ELU function is employed to distinguish the difference like this. As α_1 and α_2 increase, the ELU function approaches the ReLU function and the target property is likely to be satisfied, so relatively large values of α_1 and α_2 are used in this paper. We can see that the sensitivity of the obtained transmission property to α_1 and α_2 is not so significant from Table 3.

Table 3: Dependence of tranmission properties that may be obtained using OF2 on (α_1, α_2).

(α_1, α_2)	T_p	T_s	IR [dB]	C_{OF2}	C^*_{OF2}
(50,20)	0.75	0.009265	19.08	≃0.000	0.0
(50,20)	0.80	0.010056	19.01	≃0.000	0.0
(50,20)	0.68	0.001	28.33	≃0.000	0.0
(100,40)	0.75	0.008409	19.50	≃0.000	0.0
(100,40)	0.80	0.008976	19.50	≃0.000	0.0
(100,40)	0.69	0.001	28.39	≃0.000	0.0

References

[1] C. L. Holloway, E. F. Kuester, J. A. Gordon, J. O'Hara, J. Booth, and D. R. Smith, "An overview of the theory and applications of metasurfaces: the two-dimensional equivalents of metamaterials," IEEE Trans. Antennas Propag., vol.54, no.2, pp.10-35, Apr. 2012. DOI:10.1109/MAP.2012.6230714

[2] N. Yu, P. Genevet, M. A. Kats, F. Aieta, J. P. Tetienne, F. Capasso, and Z. Gaburro, "Light propagation with phase discontinuities: generalized laws of reflection and refraction," Science, vol.334, no.6054, pp.333-337, Sep. 2011. DOI:10.1126/science.1210713

[3] R. Izumi, S. Ikezawa, and K. Iwami, "Metasurface holographic movie: a cinematographic approach," Opt. Express, vol.28, no.16, pp.23761-23770, Aug. 2020. DOI:10.1364/OE.399369

[4] J. Sung, G. Y. Lee, and B. Lee, "Progress in the practical metasurface for holography and lens," Nanophotonics, vol.8, no.10, pp.1701-1708, Aug. 2019. DOI:10.1515/nanoph-2019-0203

[5] T. Yamamoto, A. Sanada, and H. Kubo, "Experimental verifications of left-handed characteristics of 3-D left-handed metamaterial composed of periodic wired metallic spheres," IEICE Trans. Electron., vol.E95-C, no.10, pp.1652-1657, Oct. 2012. DOI:10.1587/transele.E95.C.1652

[6] H. Kubo, K. Nishibayashi, T. Yamamoto, and A. Sanada, "New negative refractive index material composed of dielectric prisms with metal patterns," IEICE Trans. Electron., vol.E96-C, no.10, pp.1273-1280, Oct. 2013. DOI:10.1587/transele.E96.C.1273

[7] D. Schurig, J. J. Mock, B. J. Justice, S. A. Cummer, J. B. Pendry, A. F. Starr, and D. R. Smith, "Metamaterial electromagnetic cloak at microwave frequencies," Science, vol.314, no.5801, pp.977-980, Nov. 2006. DOI:10.1126/science.1133628

[8] J.B. Pendry, D. Schurig, and D. R. Smith, "Controlling electromagnetic fields," Science, vol.312, no.5781, pp.1780-1782, Jun. 2006. DOI:10.1126/science.1125907

[9] D. Schurig, J. B. Pendry, and D. R. Smith, "Calculation of material properties and ray tracing in transformation media," Opt. Express, vol.14, no.21, pp.9794-9804, Oct. 2006.

DOI:10.1364/OE.14.009794
[10] J. Li and J.B. Pendry, "Hiding under the carpet: A new strategy for cloaking," Phys. Rev. Lett., vol.101, no.20, 203901, Nov. 2008. DOI:10.1103/PhysRevLett.101.203901
[11] J. Valentine, J. Li, T. Zentgraf, G. Bartal, and X. Zhang, "An optical cloak of dielectrics," Nature Materials, vol.8, pp.568-571, Apr. 2009. DOI:10.1038/NMAT2461
[12] Y. Kato, K. Omori, and A. Sanada, "D-Band perfect anomalous reflectors for 6G applications," IEEE Access, vol.9, pp. 157512-157521, Nov. 2021. DOI:10.1109/ACCESS.2021.3130058
[13] R. Kuse, T. Hori, M. Fujimoto, T. Seki, K. Sato, and I. Oshima, "Equivalent circuit analysis of meta-surface using double-layered patch-type FSS," IEICE Trans. Commun., vol.E99-B, no.11, pp.2373-2380, Nov.2016. DOI:10.1587/transcom.2015EBP3538
[14] M. Faenzi, G. Minatti, and S. Maci,"Metasurface Antennas: Design and Performance," IEICE Trans. Commun., vol.E102-B, no.2, pp.174-181, Aug. 2018. DOI:10.1587/transcom.2018ISI0004
[15] T. B. Nguyen, N. Michishita, H. Morishita, T. Miyazaki, and M. Tadokoro, "Mantle-cloak antenna by controlling surface reactance of dielectric-loaded dipole antenna," IEICE Trans. Commun., vol.E105-B, no.3, pp.275-284, Mar. 2022. DOI:10.1587/transcom.2021EBP3026
[16] S. Chen, F. Fan, X. He, M. Chen, and S. Chang, "Multifunctional magneto-metasurface for terahertz one-way transmission and magnetic field sensing," Appl. Opt., vol.54, no.31, pp.9177-9182, Oct. 2015. DOI:10.1364/AO.54.009177
[17] Z. Tan, F. Fan, X. Dong, J. Cheng, and S. Chang, "Nonreciprocal terahertz beam steering based on magneto-optic metagratings," Sci. Rep. vol.9, 20210, Dec. 2019. DOI:10.1038/s41598-019-56789-x
[18] M. Taniguchi, A. Iguchi, and Y. Tsuji, "A study on magneto-metasurface for THz isolator ," XXXXVth URSI General Assembly and Scientific Symposium (URSI GASS), Sapporo, Japan, B07-4-3, Aug. 2023. DOI:10.23919/URSIGASS57860.2023.10265405
[19] Y. Ohkawa, Y. Tsuji, and M. Koshiba, "Analysis of anisotropic dielectric grating diffraction using the finite element method," J. Opt. Soc. Amer. A, vol.13, no.5, pp.1006-1012, May 1996. DOI:10.1364/JOSAA.13.001006
[20] Y. Ohkawa, Y. Tsuji, and M. Koshiba, "Finite element analysis of general conical diffraction by arbitrarily profiled grating," IEEE Transa. Magnetics, vol.33, no.2, pp.1440-1443, Mar. 1997. DOI:10.1109/20.582530
[21] Z.W. Geem, "Novel derivative of harmony search algorithm for discrete design variables environmental planning and management program," Appl. Math. Comput., vol.199, no.1, pp.223-230, May 2008. DOI:10.1016/j.amc.2007.09.049
[22] N. Hieda, K. Morimoto, A. Iguchi, Y. Tsuji, and T. Kashiwa, "Topology optimal design of NRD guide devices using function expansion method and evolutionary approaches," IEICE Trans. Electron., vol.E105-C, no.11, pp.652-659, Nov.2022. DOI:10.1587/transele.2021ESP0005
[23] D. Whitely, "A genetic algorithm tutorial," Statist. Comput., vol.4, pp.65-85, Jun. 1994. DOI:10.1007/BF00175354
[24] A. Koda, K. Morimoto, and Y. Tsuji, "A study on topology optimization of plasmonic waveguide devices using function expansion method and evolutionary approach," J. Lightw. Technol., vol.37, no.3, pp.981-988, Dec. 2018. DOI:10.1109/JLT.2018.2884903
[25] M.I.H. Patwary, A. Iguchi, and Y. Tsuji, "Optimal design of NRD grating bandpass filters for THz application using GA and EIM," IEEE Photon. J., vol.16, no.1, 7700109, Feb. 2024. DOI:10.1109/JPHOT.2023.3344608
[26] D. A. Clevert, T. Unterthiner and S. Hochreiter, "Fast and Accurate deep network learning by exponential linear units (ELUs)," 4th International Conference on Learning Representations (ICLR 2016), San Juan, Puerto Rico, May 2016. DOI:10.48550/arXiv.1511.07289
[27] J. Shibayama, T. Kuroda, J. Yamauchi, and H. Nakano, "Analysis of an InSb sphere array on a dielectric substrate in the THz regime," IEICE Trans. Electron., vol.E105-C, no.4, pp.159-162, Apr. 2022. DOI:10.1587/transele.2021RES0002
[28] J. Shibayama, S. Takahashi, J. Yamauchi, and H. Nakano, "Fundamental investigation of a grating consisting of InSb-coated dielectric cylinders on a substrate in the THz regime," IEICE Trans. Electron., vol.E103-C, no.11, pp.567-574, Nov. 2020. DOI:10.1587/transele.2019ESP0003
[29] M. Tomiyasu, K. Morimoto, A. Iguchi, and Y. Tsuji, "A study on function-expansion-based topology optimization without gray area for optimal design of photonic devices," IEICE Trans. Electron., vol.E103-C, no.11, pp.560-566, Nov. 2020. DOI:10.1587/transele.2019ESP0005
[30] K. Fujimoto, Y. Tsuji, K. Hirayama, T. Yasui, S. Sato, and R. Kijima, "A study on topology optimization of optical circuits consisting of multi-materials," J. Lightw. Technol., vol.30, no.13, pp.2210-2215, Jul. 2012. DOI:10.1109/JLT.2012.2195474
[31] Y. Tsuji, K. Hirayama, T. Nomura, K. Sato, and S. Nishiwaki, "Design of optical circuit devices based on topology optimization," IEEE Photon. Technol. Lett., vol.18, no.7, pp.850-852, Apr. 2006. DOI:10.1109/LPT.2006.871686

Mio Taniguchi received the B.S. in electronic engineering and M.S. degrees in department of nano-structures and advanced materials from Kagoshima University in 2002 and 2008, respectively. From 2008 to 2019, she was with Opnest Japan, Inc., where she was engaged in research on design and development of semiconductor lasers, manufacturing technology and inventions. From 2019 to 2022, She was a researcher at Muroran Institute of Technology, where she was engaged in research on effective use of frequencies in unmanned aerial vehicle out-of-sight flights. She is currently studying toward the Ph.D. degree of engineering in Muroran Institute of Technology. Ms. Taniguchi is a student member of the Institute of Electronics, Information and Communication Engineers (IEICE). In 2021, she recieved the Best Paper Award at IEEE International Symposium on Antennas and Propagation (ISAP).

Akito Iguchi received the B.S., M.S., and Ph.D. degrees in electronic engineering from Muroran Institute of Technology, Muroran, Japan, in 2015, 2017, and 2019, respectively. From 2019 to 2020, he was a Post-Doctoral Research Fellow of Japan Society for the Promotion of Science (JSPS). He is currently an Assistant Professor at Muroran Institute of Technology. Dr. Iguchi is a member of the Institute of Electronics, Information and Communication Engineers (IEICE), the IEEE, and the Optica. In 2020, he recieved Young Researcher's Award from IEICE.

Yasuhide Tsuji received the B.S., M.S., and Ph.D. degrees in electronic engineering from Hokkaido University, Sapporo, Japan, in 1991, 1993, and 1996, respectively. In 1996, he joined the Department of Applied Electronic Engineering, Hokkaido Institute of Technology, Sapporo, Japan. From 1997 to 2004, he was an Associate Professor of Electronics and Information Engineering at Hokkaido University. From 2004 to 2011, he was an Associate Professor of Electrical and Electronic Engineering at Kitami Institute of Technology, Kitami, Japan. Since 2011, he has been a Professor of Information and Electronic Engineering at Muroran Institute of Technology, Muroran, Japan. He has been interested in wave electronics. Dr. Tsuji is a Senior Member of the Institute of Electronics, Information and Communication Engineers (IEICE), the IEEE, and the Optica, and a Member of the Japan Society of Applied Physics. In 2021, He has received the Electronics Society Award form IEICE. In 1997, 1999, and 2019, he was awarded the Best Paper Award from IEICE. In 2000, he has received the Third Millennium Medal from IEEE. In 2019, he has received the IEEE Photonics Technology Letters Outstanding Reviewer Award.